Nat. Hazards Earth Syst. Sci. Discuss., https://doi.org/10.5194/nhess-2018-109
Manuscript under review for journal Nat. Hazards Earth Syst. Sci.
Discussion started: 12 June 2018

Natural Hazards and Earth System Sciences
Discussions

How size and trigger matter: analyzing rainfall- and earthquake-triggered landslide inventories and their causal relation in the Koshi River basin, Central Himalaya

Jianqiang Zhang [1,2], Cees J. van Westen [2], Hakan Tanyas [2], Olga Mavrouli [2], Yonggang Ge [1], Samjwal Bajrachary [3], Deo Raj Gurung [3], Megh Raj Dhital [4], Narendral Raj Khanal[5]

[1]Key Laboratory of Mountain Hazards and Surface Process/Institute of Mountain Hazards and Environment, Chinese Academy of Sciences, Chengdu, China.

[2]Faculty of Geo-Information Science and Earth Observation (ITC), University of Twente, the Netherlands.

[3]International Centre for Integrated Mountain Development (ICIMOD), Lalitpur, Nepal.

[4]The Department of Geology, Tri-Chandra Multiple Campus, Ghantaghar, Kathmandu, Nepal.

[5]Central Department of Geography, Tribhuvan University, Kathmandu, Nepal.

Correspondence to: Jianqiang Zhang(zhangjq@imde.ac.cn)

Abstract: Inventories of landslides caused by different triggering mechanisms, such as earthquakes，extreme rainfall events or anthropogenic activities, may show different characteristics in terms of distribution, causal factors and frequency-area relationships. The aim of this research is to study such differences in landslide inventories, and the effect they have on landslide susceptibility assessment. The study area is the watershed of the trans-boundary Koshi River in central Himalaya, shared by China, Nepal and India. Detailed landslide inventories were generated based on visual interpretation of remote sensing images and field investigation for different time periods and triggering mechanisms. Maps and images from the period 1992 to 2015 were used to map 5,858 rainfall-triggered landslides and after the 2015 Gorkha earthquake, an additional 1138 co-seismic landslides were mapped. A set of topographic, geological and land cover factors were employed to analyze their correlation with different types and sizes of landslides. The results show that the frequency - area distributions of rainfall and earthquake–triggered landslides varied considerably, with the former one having a larger frequency of small landslides. Also topographic factors varied considerably for the two triggering events, with both elevation and slope angle showing significantly different patterns for earthquake-triggered and rainfall-triggered landslides. Landslides were classified into two size groups, in combination with the main triggering mechanism (rainfall- or earthquake-triggered). Susceptibility maps for different combinations of landslide size and triggering mechanism were generated using logistic regression analysis. The different triggers and sizes of landslide data were used to validate the models. The results showed that susceptible areas for small and large size rainfall- and earthquake-triggered landslides differed substantially, while susceptibility maps for different size of earthquake-triggered landslides were similar.

Key words: landslides, rainfall-triggered, earthquake-triggered, frequency-area analysis, susceptibility assessment,

Nepal

1. Introduction

Landslides are one of the most harmful geological hazards causing substantial fatalities and loss of property worldwide, affecting settlements, agriculture, transportation infrastructure and engineering projects (Dilley et al. 2005; Petley, 2012; Zhang et al., 2015; Haque et al., 2016). Among the various characteristics that determine the potential damage of landslides, size plays an important role, as well as velocity, depth, impact pressure, or displacement which differs for the various mass movement types. Volume may be an even more important landslide characteristic than size, but this is difficult to measure as it requires specific geophysical or geotechnical methods that can be applied at a site investigation level, or the use of multi-temporal Digital Elevation Models (SafeLand, 2015; Martha et al., 2017). Therefore, empirical relations between landslide area and volume are generally used (Dai and Lee, 2001; Guzzetti et al., 2008; Larsen et al., 2010; Klar et al., 2011; Larsen and Montgomery, 2012). To investigate whether earthquake- and rainfall-triggered landslides inventories have similar area-frequency distributions, area-volume relations and spatially controlling factors, it is important to collect event-based landslide inventories. The difficulty is to collect complete inventories that are independent for earthquakes and rainfalls.

Many studies that compare the characteristics of earthquake- and rainfall-triggered landslide inventories focus on mapping landslides triggered by rainfall after major earthquakes. For example, Lin et al. (2006) and Chang et al. (2007) studied the difference between earthquake- and typhoon-triggered landslides in mountainous watersheds in Taiwan. Landslides were mapped from eight satellite images covering a period between 1996 and 2001 and concluded that the density of rainfall-triggered landslides increased significantly after the earthquake, and the places where landslides occurred changed, and concluded that different triggers produced significantly different patterns, with rainfall-triggered landslides occurring more near channels and earthquake-triggered ones close to ridges. Menuier et al. (2008) compared rainfall-triggered landslides in the western Southern Alps of New Zealand with some earthquake-triggered landslides, and found that the rainfall-triggered landslides were evenly distributed over all slope segments, and the landslide susceptibility was lower near ridge crests. Tang et al. (2011) mapped landslides in the Beichuan area after the 2008 Wenchuan earthquake in China. They mapped 2221 co-seismic landslides but also 696 rainfall-triggered landslides which occurred several months later, and which were located in the same area, as most of them were reactivations of the co-seismic landslides. Tang et al. (2016) analyzed changes in landslide activity near the epicenter of the 2008 Wenchuan earthquake by generating five landslide inventories for different years through stereoscopic digital visual image interpretation. From May 2008 to April 2015, 660 new landslides occurred outside the co-seismic landslide areas. In April 2015, the number of active landslides had gone down to 66, less than 1% of the co-seismic

landslides, still much higher than the pre-earthquake situation. The problem with the studies indicated above is that rainfall-triggered landslides that occur shortly after a major earthquake are generally following the same patterns, due to the availability of large volumes of landslide materials of the co-seismic landslides. There are fewer studies that compare the two triggering mechanisms in an independent manner.

Landslide susceptibility assessment is carried out to define the landslide-prone areas depending on potential causal factors (or internal factors that make certain areas susceptible to landslides) and triggering factors (which are external dynamic factors which initiate the landslide event). In medium and regional scale landslide susceptibility assessment, statistical methods are commonly used (Carrara et al. 1995; Soeters and van Westen 1996; Chung and Fabbri 1999; Guzzetti et al. 1999; Duman et al. 2006; Bathrellos et al. 2009). Causal factors generally include topographical factors (slope gradient, elevation difference, slope aspect etc.), geological factors (lithology, joints, faults, etc.) and land use factors (current land use, land use changes, slope cuts etc.) (Kamp et al. 2008). The spatial representation of dynamic triggering factors is often complicated to analyze (e.g. topographic amplification and peak ground acceleration during earthquakes or water tables during extreme rainfall events) because of the large uncertainty of soil depth and soil conditions over certain areas. Therefore these triggering factors are often not included within landslide susceptibility assessment. As historical evidence is a key input in the prediction of future landslide events, landslide inventories are one of the most important inputs in statistical landslide susceptibility assessment. However, complete inventories are scarce, and landslide inventories often reflect the results of the last triggering event (van Westen et al. 2008).

There is no clear evidence shows the difference on morphology between rainfall-triggered landslide and earthquake-triggered landslide. But some statistics on landslides with causal factors show the difference induced by different triggers. Fan et al. (2012) found that, when volume smaller than $10\times10^4 m^3$, both rainfall-triggered landslide and earthquake-triggered landslide have similar distance of runout; when volume larger than$10\times10^4 m^3$, the earthquake-triggered landslide has longer runout than rainfall-triggered landslide. Different size of landslide show different characteristics. The large size landslides can generate high speed and long distance hazard due to the wide range of instability area and huge potential energy. Korup et al. (2007) found that relative relief and rock strength are the significant factors to affect the occurrence of large size landslides. Peng et al. (2014) analyzed the landslides in the Three Gorges area and found that medium size and large size of earth slides are located in a wide range of elevation, as well as large size rock slides; Most small size, large size and huge size of rock slides are located in north slopes; medium and large size landslides mostly occur at shale, sandstone and mudstone and other soft stratum, as well as carbonate rock and clastic rock interbedded stratum.

The first question that will be addressed in this research is whether it is possible to utilize inventories of earthquake-triggered landslides (ETL) as inputs for analyzing the susceptibility of rainfall-triggered landslides (RTL). Although landslide size is often considered important in hazard assessment and risk assessment, it is generally not considered as

a separate component of the susceptibility assessment. The second question that will be investigated in this study is whether different landslide size groups are controlled by different sets of causal factors.

The aim of this study is to investigate the differences in the mappable characteristics of earthquake-triggered and rainfall triggered landslides in terms of their frequency-area relationships, spatial distributions and relation with causal factors, and to evaluate whether separate susceptibility maps generated for specific landslide size and triggering mechanism are better than a generic landslide susceptibility assessment including all landslide sizes and triggers.

2. Study area

The study was carried out in the Koshi River basin, which is a trans-boundary basin located in China, Nepal and India in the central Himalayas (Fig. 1a). The mountainous regions in the upper reaches of the basin where landslides have occurred are located in China and Nepal, and the Indian part consists of relatively flat areas. The elevation of Koshi River basin varies from 60 m a.s.l. at the outlet in India up to 8,844 m at the highest point at Mount Everest. The Koshi basin can be classified into 6 physiographic zones from South to North: Terai, Siwalik Hills, Mahabharat Lekh, Middle Mountains, High Himalaya，and Tibetan Plateau (Gurung and Khanal 1987; Dhital 2015). Considering the distribution of landslides, the Tibetan plateau in the upper reaches and the plains in the lower reaches were excluded.

In the Koshi Basin, the major geological structures have an approximate east–west orientation, such as the foreland thrust-fold belt, Main Central Thrust (MCT), South Tibetan Detachment System (STDS) and the Yarlung Zangbo Suture Zone (YZSZ) (Gansser, 1964; Dhital，2015). The southernmost part of the basin consists of the Quaternary sediments underlain by the Neogene Siwaliks. The Siwaliks comprise soft mudstones, sandstones and conglomerates. In this part of the foreland basin, a number of emergent and blind imbricate faults originate from the Main Himalayan Thrust. The overlying Lesser Himalayan succession forms duplexes and imbricate stacks. The Proterozoic to Miocene rocks of the Lesser Himalaya include limestones, dolomites, slates, phyllites, schists, quartzites, and gneisses (Dhital, 2015). A regional-scale thrust MCT separates the Lesser Himalayan sequence from the overlying Higher Himalayan crystallines, which consist of medium- to high-grade metamorphic rocks (e.g., schists, quartzites, amphibolites, marbles, gneisses, and migmatites) and granites aged from the Proterozoic to Miocene. The STDS delineates the Higher Himalayan rocks from the overlying Tethyan sedimentary sequence of Paleozoic–Cenozoic age (Gansser, 1964; Burg et al., 1984; Hodges et al., 1996) (Fig. 1b).

In the study area there are three main tributaries of the Koshi River: the Arun (main branch) coming from the north, the Sun Koshi from the west and Tamor from the east. Nearly every year, during the monsoon period, which generally lasts from June to September, the area is affected by rainfall-triggered landslides. Dahal and Hasegawa (2008) used a dataset of 193 landslides occurring from 1951 to 2006, part of which were from the Koshi River basin, to generate a

Nat. Hazards Earth Syst. Sci. Discuss., https://doi.org/10.5194/nhess-2018-109
Manuscript under review for journal Nat. Hazards Earth Syst. Sci.
Discussion started: 12 June 2018

Natural Hazards and Earth System Sciences
Discussions

threshold relationship between rainfall intensity, rainfall duration, and landslide initiation.

The area was severely affected by the Gorkha earthquake, with a moment magnitude of 7.8 on 25 April 2015. The epicenter was located near Gorkha, which is about 80km west of the study area. A second major earthquake occurred along the same fault on 12 May 2015 with a moment magnitude of 7.3 with the epicenter located inside the Koshi River basin. The second event is considered as a major aftershock of the main Gorkha earthquake. Both events triggered many landslides (Collins and Jobson 2015; Kargel et al. 2016; Zhang et al. 2016; Martha et al. 2017).

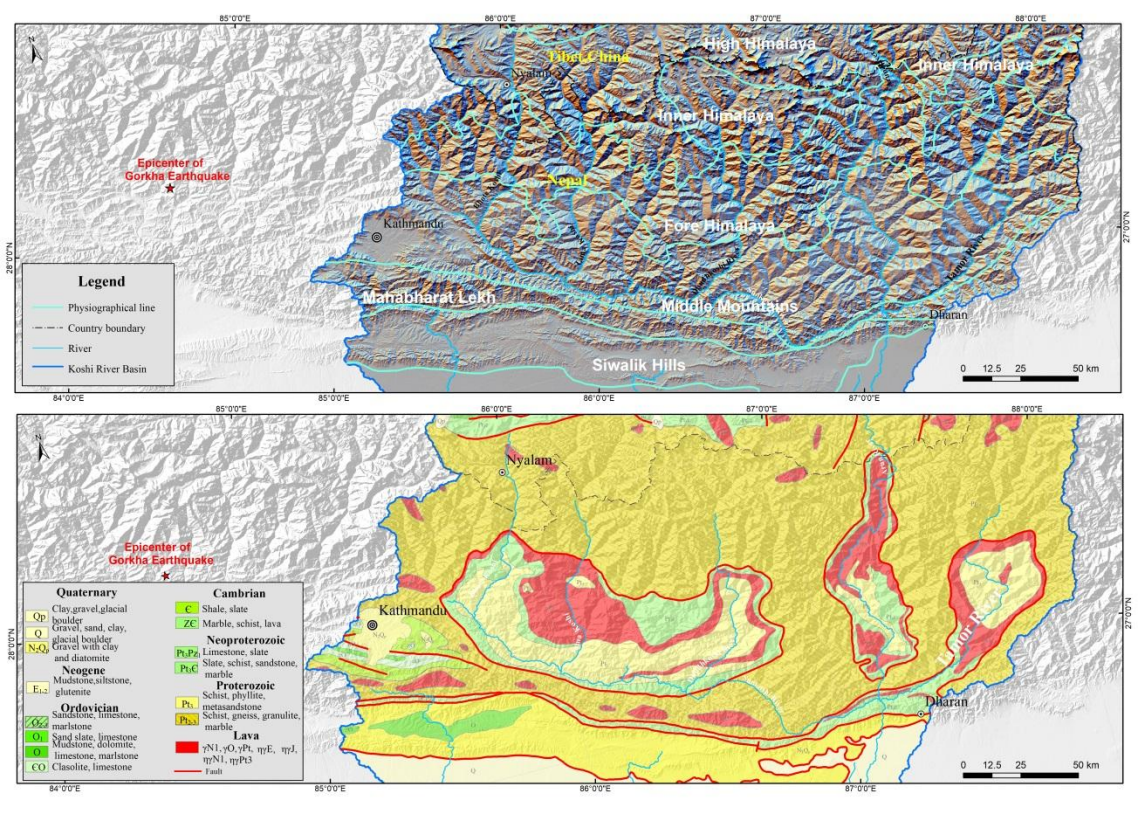

Fig. 1 Maps showing the study area (a) Physiographic zones of the Koshi River basin; (b) Geological map showing the main geological zones (Dhital, 2015; Zhang et al. 2016).

3. Input data

The study requires a series of landslide inventory maps, and causal factor maps, which were generated for the middle part of the Koshi basin, where most of the landslides were concentrated. Two landslide inventories were generated: a pre-2015 inventory showing rainfall-triggered landslides, and a co-seismic landslide map for the 2015 Gorkha earthquake. The pre-2015 inventory map was generated using topographic maps, Google Earth and Landsat ETM/TM

images. We were able to digitize landslide polygons from the available 1:50,000 scale topographic maps, which cover only the Nepalese part of the Koshi River basin. These maps were generated from aerial photographs acquired in 1992, and landslides were marked as separate units. The smallest landslide with area of 456.6 m^2 was identified. More recent landslides were mapped from Google Earth images which were captured during Feb. 2015(Some images were captured in Dec. 2014), using visual image interpretation and screen digitizing. Google Earth supplies high resolution remote sensing imageries from different years, on which even small landslides can be recognized. Landsat ETM imageries and ASTER DEM data were therefore used to adjust the location of the landslides. Landslides with area larger than 50 m^2 could be recognized by this method. A total of 5,858 rainfall induced landslides were identified in the Koshi River basin.

After the 2015 April 25th Gorkha earthquake, it was possible to use images from the Chinese GaoFen-1 and GaoFen-2 high resolution satellites of the CNSA (China National Space Administration), which are part of the HDEOS (High-Definition Earth Observation Satellite) program. These images were captured during 27 April, 2015 to May 14 2015. After the earthquake some rainfalls occurred, and the coming monsoon brought more rainfall in earthquake-affected area. There could be some changes for earthquake-triggered landslide which were impossible to be modified. We tried to use the images captured very close to earthquake time in order to reduce the impact by rainfall to landslide after the earthquake. By comparing with images before the earthquake, as well as rainfall-triggered landslide inventory, earthquake-triggered landslides were mapped as polygons, without separating erosion, transportation and accumulation parts, and without a classification in landslide types.

For the susceptibility assessment, points located in the source area of landslides, were used as indicative of the initiation conditions.

The SRTM Digital Elevation Model with 90m spatial resolution was used in this study. ESRI ArcGIS software enabled the calculation of topographical factors including slope gradient, aspect, curvature, and distance to rivers. The land cover dataset GlobeLand30 with 30×30m spatial resolution, developed by the National Geomatics Center of China, was employed in this study. The land cover types include cultivated land, forest, grassland, shrub land, wetland, water bodies, tundra, artificial surfaces and bare land. Geological maps of Nepal, and Tibet were obtained from Chengdu Geological Survey Center of the China Geological Survey. The Peak Ground Acceleration data for the Gorkha earthquake were obtained from USGS.

4. Methods

Figure 2 gives an overview of the method followed in this study The landslide inventories were subdivided into training and test datasets. For each group 60% of the landslide data were used for the modeling, and 40% of the data were used for the validation. Based on the frequency area distribution the RTL and ETL inventories were separated in

two size-groups each. Initially bivariate statistical analysis was used for the different types and sizes of landslides, to investigate the correlation between landslides with causal factors. After selecting the relevant factors, the logistic regression method was used to build the susceptibility model for each size group. The logistic regression method is the most commonly used model in landslide susceptibility assessment (Ayalew and Yamagish 2005; Bai et al. 2010; Das et al. 2010; Nandi and Shakoor 2010; Wang et al. 2013). For the susceptibility modeling of RTL, the following factors were used: elevation (x_1), slope gradient (x_2), curvature (x_3), slope aspect (x_4), relative relief (x_5), drainage density (x_6), lithology (x_7), distance to faults (x_8) and land cover type (x_9). For the susceptibility modeling of ETL, peak ground acceleration (x_{10}) was added. The R software was used to build the models for different types and sizes of landslide respectively. ROC (Receiver Operating Characteristic) curves were used to verify the accuracy of the susceptibility models, and finally six landslide susceptibility maps were generated and compared (Fig. 2).

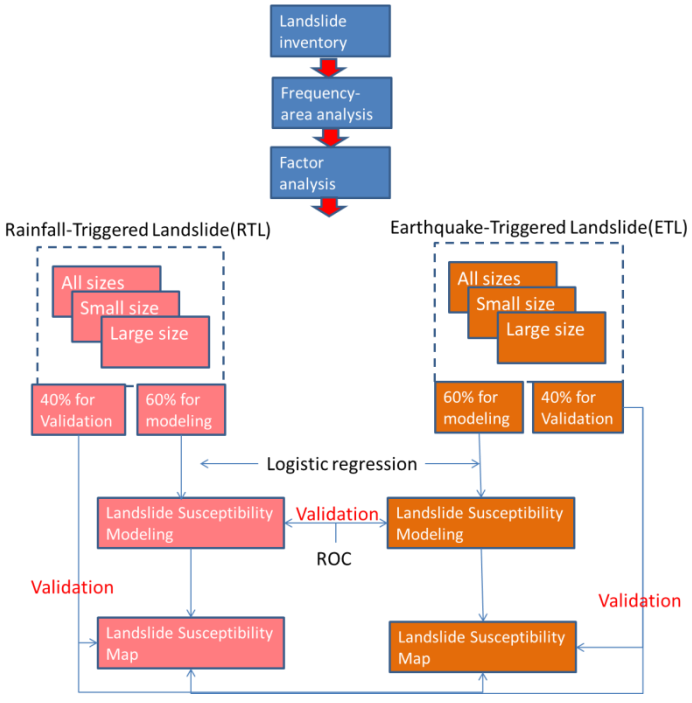

Fig. 2 Methodology for susceptibility assessment to different types and sizes of landslide

5. Landslide characteristics

In the Koshi River basin, a total of 5,858 RTL were mapped. The Gorkha earthquake triggered more than 3000 landslides, of which 1,138 are located in the Koshi River basin. Landslide characteristics were analyzed based on frequency-area distribution and factor statistics (Fig. 3).

Nat. Hazards Earth Syst. Sci. Discuss., https://doi.org/10.5194/nhess-2018-109
Manuscript under review for journal Nat. Hazards Earth Syst. Sci.
Discussion started: 12 June 2018

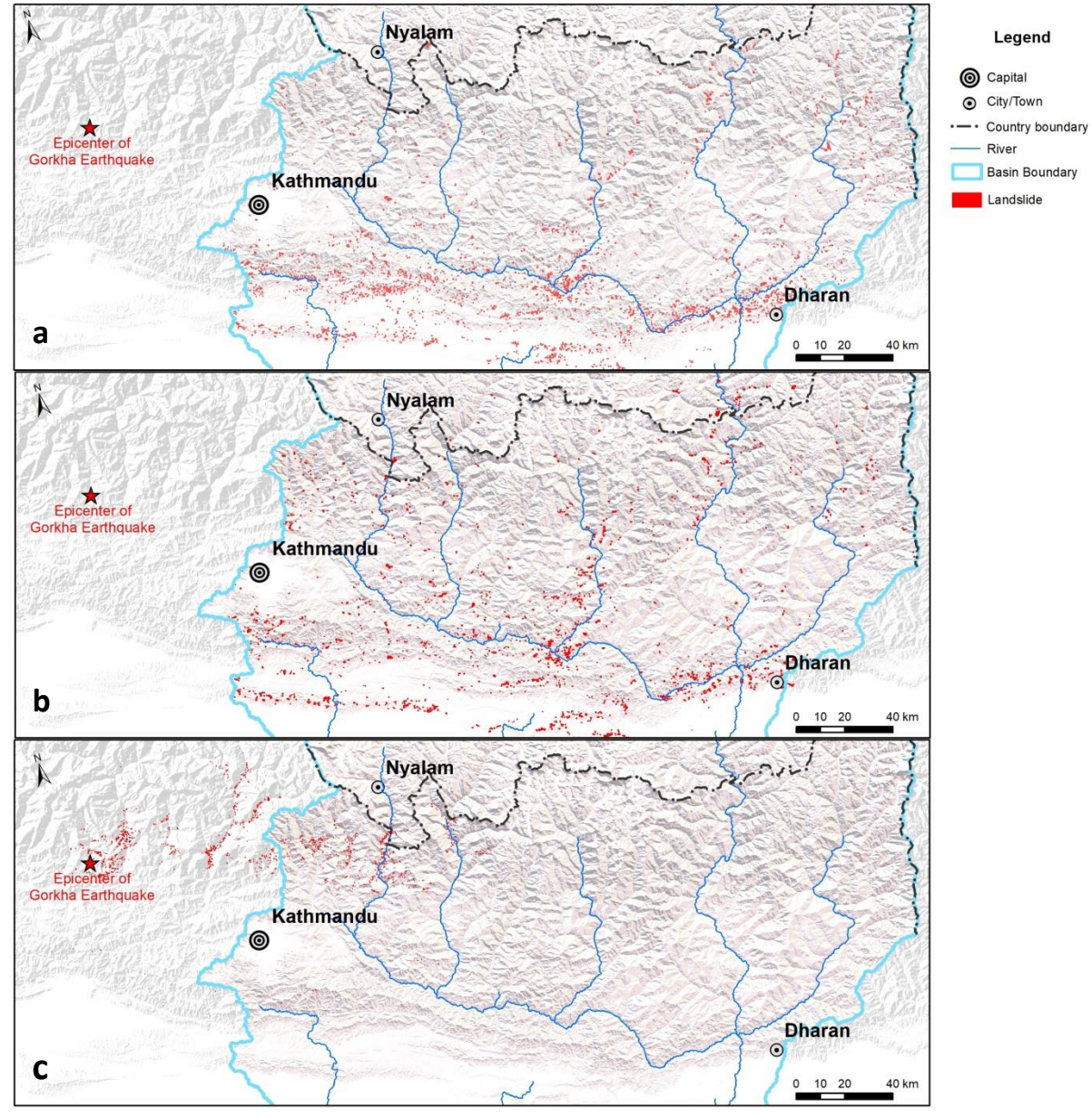

Fig. 3 Landslide inventory of Koshi River basin (a) Landslide inventory of RTL before 1992; (b) Landslide inventory of RTL in 1992~2015; (c) Landslide inventory of ERL by Gorkha earthquake.

5.1 Landslide frequency-area distributions

The frequency-area distributions (FAD) of landslides were separately analyzed for both RTL and ETL inventories (Fig. 4). For the RTL both landslide inventory data before 1992 and 1992~2015 were analyzed. For the ETL of the Gorkha

earthquake, landslides located in the Koshi River basin were analyzed separately from the entire ETL inventory. Malamud et al. (2004) examined the FAD of landslides and quantified the landslide triggering event with a parameter called landslide magnitude (mL). In a similar manner, we estimated a mL between 4.0 and 4.5 for the ETL inventory. If we compare this with the mL of other inventories, we can conclude that this landslide inventory has a landslide magnitude scale similar to the landslides triggered by the 1994 Northridge event (Harp and Jibson 1995), of 4.0 mL approximately (Malamud et al. 2004), but lower than the landslide event magnitude of the Wenchuan earthquake which varies between 4.96 and 6.24, depending on the inventory used (Tanyas et al. 2017). The β values were obtained as 2.44 and 2.38 for the RTL in 1992 and 2010, and 2.40 and 2.87 for all ETL of the Gorkha earthquake and those only within the Koshi River basin. The cut-off values (which are the landslide areas below which the FAD is no longer having a powerlaw relation) were 25,000 - 30,000 m^2 for RTL and 5,000 - 6,600 m^2 for all ETL.

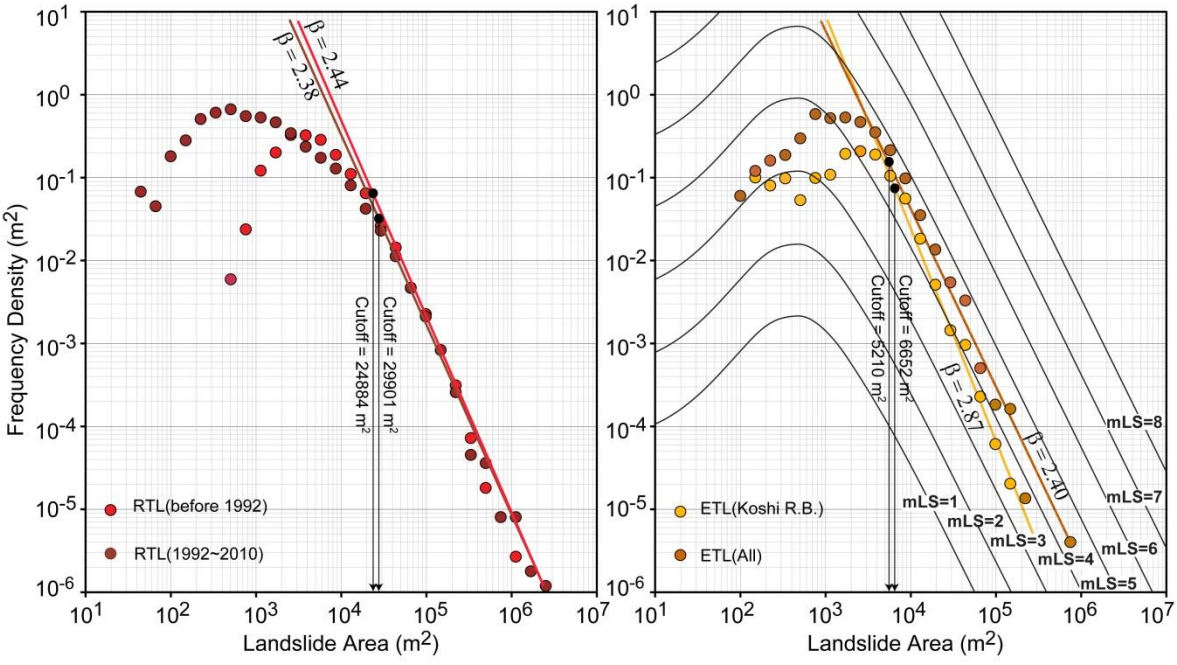

Fig. 4 Landslide frequency - area analysis in Koshi River basin (a): RTL; (b): ETL.

Landslide size classification proposed by Tong (2013) was referenced, where landslides with an area smaller than 1000 m^2 were classified as small, those with an area between 1,000 m^2 and 10,000 m^2 as medium, and those with larger sizes than 100,000 m^2 as large size landslides. Based on the results of the FAD analysis, as well as field experience, the RTL and ETL inventories were subdivided according to landslide size. In order to facilitate the analysis, we subdivided them into two size-groups, with 6,000 m^2 as boundary value. Landslide data were organized into 6 groups based on

Nat. Hazards Earth Syst. Sci. Discuss., https://doi.org/10.5194/nhess-2018-109
Manuscript under review for journal Nat. Hazards Earth Syst. Sci.
Discussion started: 12 June 2018

the two triggers (rainfall and earthquake) and two size classes (Table 1).

Table 1 Numbers for different types and sizes of landslide in Koshi River basin

	Rainfall-triggered landslides (RTL)			Earthquake-triggered landslides (ETL)		
	All sizes	Small size	Large size	All sizes	Small size	Large size
Total	5,858	2,995	2,863	1,138	852	286
Modelling	3,515	1,797	1,718	682	511	171
Validation	2,343	1,198	1,145	456	341	115

5.2 Correlation of landslides with causal factors

Many factor pairs were analyzed using bivariate statistical analysis, and five causative factors that had the highest correlation with landslides were selected for the final analysis: elevation, slope gradient, slope aspect, distance to fault and lithology. The results are summarized in Fig. 5.

Statistical analysis was performed for the different size groups of ETL and RTL considering combinations of elevation and slope gradient and the results (Fig. 5a&b) indicate that, RTL are more frequent at lower altitude, especially in the Siwaliks. The numbers of landslide become very small when the altitude higher than 2000 m. ETLs are more frequent in higher elevation, related to the elevation of the blind thrust triggering the earthquake, most of them located in the area with altitude higher than 2000 m. When comparing the size groups it is also clear that small RTLs occur relatively more at lower elevation and less steep slopes than larger RTLs. For ETLs there is no clear differentiation between elevation and slope relations for the two size groups. This may be affected by the types of landslides. Most of the ETLs consist of rockfalls and rockslides which occur in higher and steeper rocky slopes, whereas most RTLs are debris slides located on gentler slopes with soil deposits.

Nat. Hazards Earth Syst. Sci. Discuss., https://doi.org/10.5194/nhess-2018-109
Manuscript under review for journal Nat. Hazards Earth Syst. Sci.
Discussion started: 12 June 2018

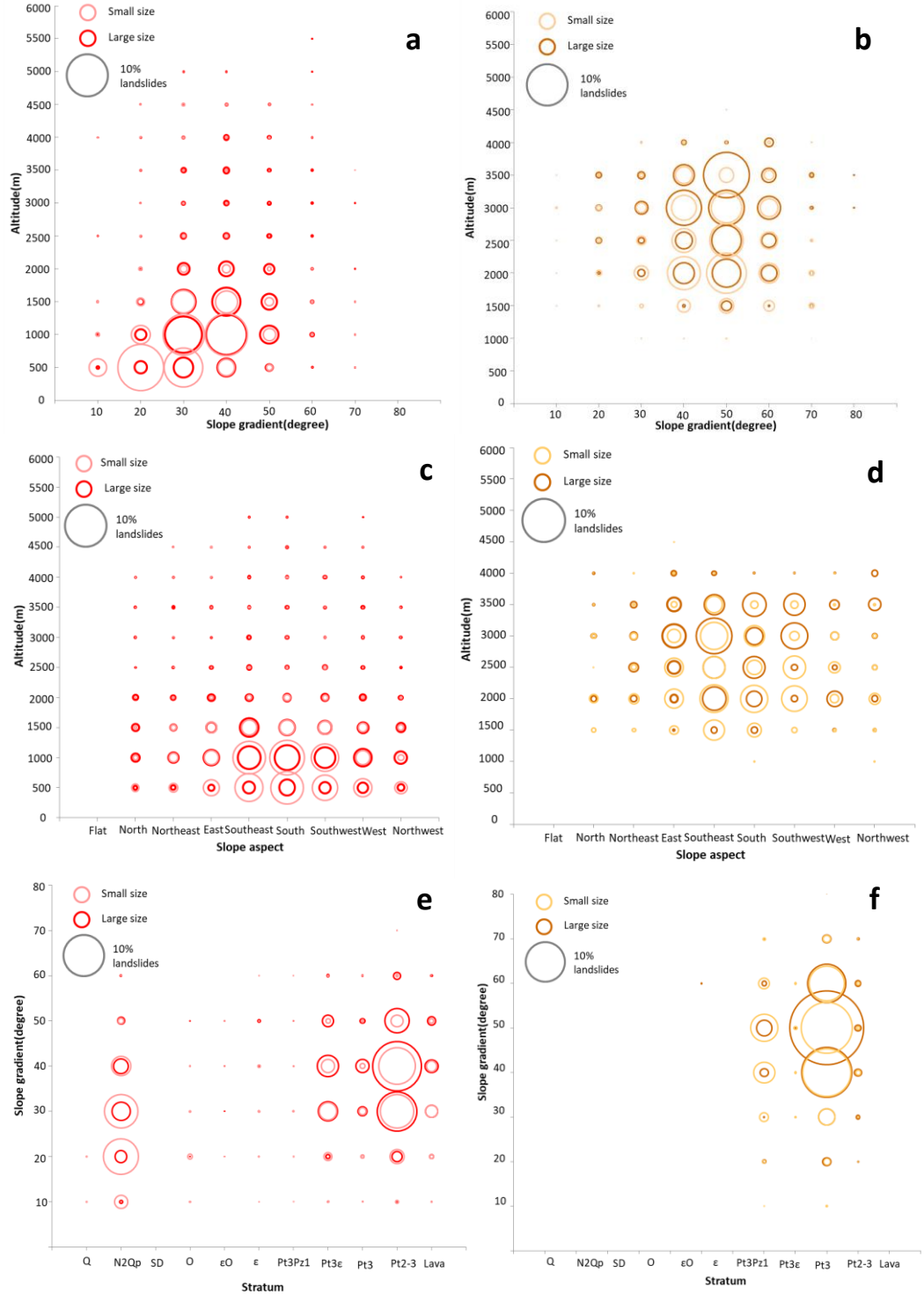

Fig. 5 Correlation between landslides and other factors for rainfall triggered landslides (RTL) on the left side, and

238 earthquake-triggered landslides (ETL) on the right side. The gray circle shows size for 10% of landslides. a & b:
239 Relation between elevation and slope gradient; c & d: Relation between slope direction and elevation; e & f: Relation
240 between Lithology and slope gradient.
241
242 The slope aspect may have an effect on the occurrence of landslides by influencing the rock weathering, snow melting,
243 and land cover, as well as the transmission of seismic waves(Kamp et al. 2008). Fig. 5 c&d show the correlation
244 between landslides, altitude and slope aspect. The majority of RTLs is located on slopes directed to the . In different
245 altitude, RTLs show the same relationship with slope aspect. These slope aspects are windward slope with more
246 precipitations, which supply the trigger for landslides. Most of ETLs are also distributed in south, southeast or
247 southwest slopes, but with increasing of altitude, the relatioship with slope aspect changes. The comparison of the size
248 groups showed that, most large size ETLs are located on south and southwest facing slopes with high elevation, while
249 more small-size ETLs are located in similar slope directions but in relatively lower elevations (Fig. 5 c&d).
250 Fig. 5e&f show the relation with slope and lithology. RTLs are concentrated on Proterozoic metamorphic lithological
251 units (Pt_{2-3}), consisting of schist, gneiss, and marbleand in Quanternary molasse (N_2Qp) unitws (See Fig. 1). The Pt_{2-3}
252 unit contains landslides of both size classes located in the steeper slopes with gradient of 20°-40°, while in the unit
253 N_2Qp, more landslides are located in gentler slopes with gradient 10°-30°. The statistics also showed that, in the unit of
254 N_2Qp with weaker rocks there were more small size landslide, and in the unit of Pt_{2-3} with stronger rocks there are
255 more large size landslides.
256 ETLs also concentrated on Pt_{2-3}, but more ETL are located in steeper slopes. The percentages for large size and small
257 size of ETL are similar in different slope interval except in slopes of 40° -50°, where more large size landslide have
258 occured.
259
260
261 **6. Landslide susceptibility assessment**
262 6.1 Landslide susceptibility models
263 For the susceptibility modeling of RTL, the contributing factors include: elevation(x_1), slope gradient(x_2),
264 curvature(x_3), slope aspect(x_4), relative relief(x_5), gully density(x_6), lithology(x_7), distance to fault(x_8) and land cover
265 type(x_9). The Peak Ground Acceleration, PGA, (x_{10}) was added to the assessing factors for the susceptibility modeling
266 of ETL. The R software was used to build the models for different types and sizes of landslide respectively (Table 2).
267 Weight of landslide susceptibility models show differences between different triggers and different sizes of landslides.
268 Altitude, curvature and slope gradient with weights of -7.5456, -6.2341 and 6.1481 respectively have high impact on
269 susceptibility of RTL, while relative relief, curvature and slope gradient with weights of 24.4495, -22.4360 and 8.7348

have high impact on susceptibility of ETL. Factors of curvature and relative relief show differences for small size and large size of RTL; elevation and curvature were very different between small size and large size of ETL.

Table 2 Susceptibility models for different triggers and sizes of landslide in Koshi River basin

Landslide type	x_1	x_2	x_3	x_4	x_5	x_6	x_7	x_8	x_9	x_{10}	p	AUC
All RTL	-7.5457	6.1481	-6.2341	-0.1131	-2.3020	-0.6447	1.3392	-0.4253	1.1421	-	2.8968	0.820
Small size RTL	-9.5260	6.1132	-12.0070	-0.2230	-6.1225	-2.0765	1.4518	-0.9228	-0.9673	-	9.4669	0.809
Large size RTL	-7.16699	6.20998	-5.12041	0.10008	2.13507	-0.23847	0.95660	-0.01205	1.58680	-	1.21971	0.852
All ETL	-1.5853	8.7368	-22.4360	-0.1432	24.4495	5.9713	2.4447	0.2831	0.9352	5.5455	5.9066	0.940
Small size ETL	-0.85231	8.07288	-32.9325	0.06238	23.9783	5.31668	2.46812	0.34372	1.15004	5.66908	13.3380	0.941
Large size ETL	-4.0451	8.3146	-11.9824	0.3314	25.3506	3.5029	2.7321	-0.4193	-0.7274	6.5423	-1.0992	0.940

6.2 Result

The logistic regression models were applied to the Koshi River basin, and in total six susceptibility maps were generated (Fig. 6). Susceptibility values were classified into four levels: low, moderate, high and very high, based on the following susceptibility threshold values: 0-0.25, 0.25-0.5, 0.5-0.75 and 0.75-1.

The RTL susceptibility map (Fig. 6a) shows that high and very high susceptible are located mostly in the Siwaliks and in the Mahabharat Lekh region in west-eastern direction and the Middle to High Himalaya region in north-south direction. The Siwaliks and Mahabharat Lekh regions have high and very high susceptibility levels for small landslides, and lower susceptibility levels for large ones. The Middle and High Himalaya region has a reverse situation: high and very high susceptibility levels for large landslides, and lower levels for small ones.

The ETL susceptibility map reflects the co-seismic landslide pattern of the Gorkha earthquake, with very high and high susceptibility in the western part of the Koshi. It is important to note that the ETL susceptibility map only reflects the characteristics of the Gorkha earthquake and is therefore not a reliable map for future earthquakes that may have another epicentral location, length of fault ruptures and magnitudes.

There is no much difference between susceptibility maps for small size ETL and large size ETL. First hand, this may be due to the far distance to the earthquake epicenter. The earthquake has low impact to the large size ETL. From the study on ETL by the 2008 Wenchuan earthquake, the study showed that 80% of large size landslide concentrated in the distance less than 5 km to the main faults (Xu and Li 2010). Second hand the large size ETL may relate to other factors including secondary faults, rock structure, which need more detail information.

Nat. Hazards Earth Syst. Sci. Discuss., https://doi.org/10.5194/nhess-2018-109
Manuscript under review for journal Nat. Hazards Earth Syst. Sci.
Discussion started: 12 June 2018

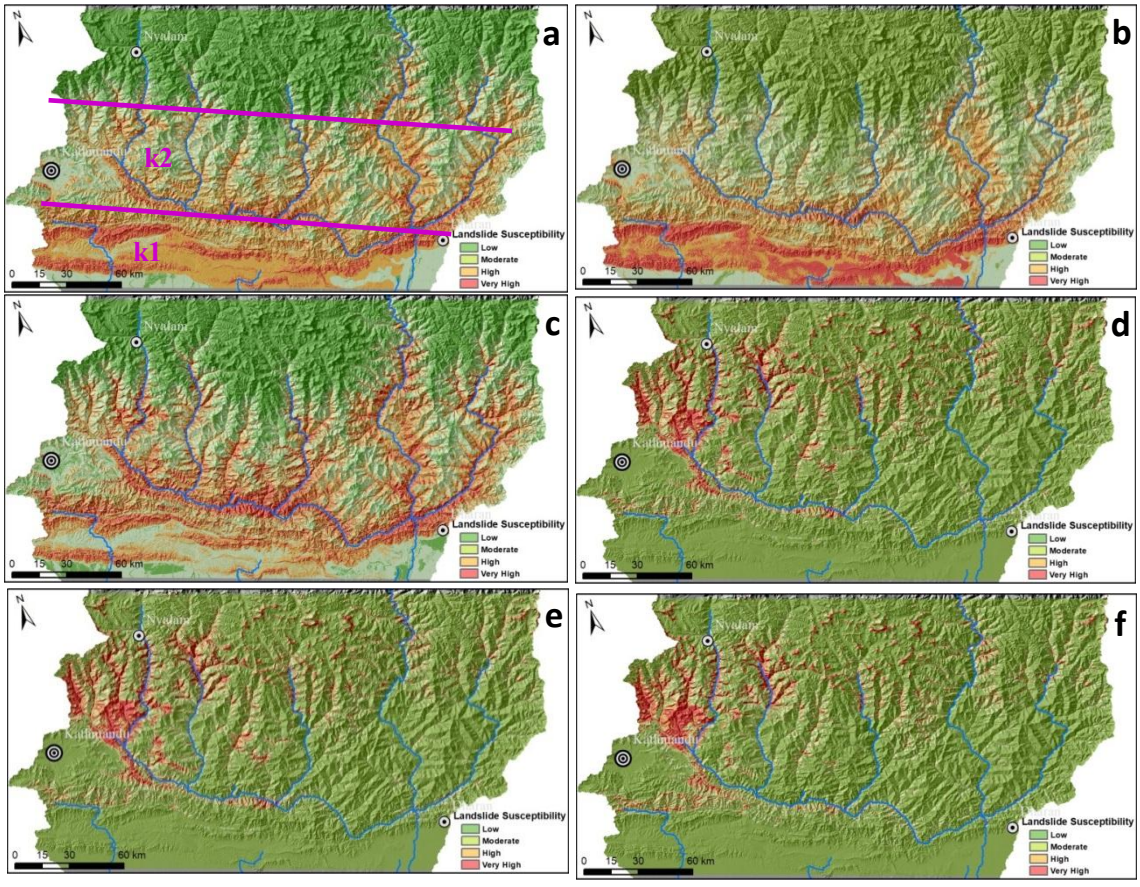

Fig. 6 Susceptibility maps for different sizes of RTL and ETL: (a) for all RTLs; (b) for small RTLs; (c) for large RTLs; (d) for all ETLs; (e) for small ETLs; (f) for large ETLs.

The areal coverage of the different levels of landslide susceptibility was calculated for each susceptibility map (Fig. 7). Compared to RTL, the ETL susceptibility maps have a larger area with low susceptibility, due to fact that the Koshi River basin is far from the epicenter of Gorkha earthquake, thus the earthquake affected region is not large. The very high and high susceptible region for ETL is mostly concentrated in the southern part of the basin. Thus it can be concluded that rainfall has a wider and stronger effect on landslide occurrence than the Gorkha earthquake in Koshi River basin.

The very high and high susceptibility areas for large size ETLs is larger than small size ETLs, while the very high and high susceptible area for large size RTL is smaller than small size RTL.

Nat. Hazards Earth Syst. Sci. Discuss., https://doi.org/10.5194/nhess-2018-109
Manuscript under review for journal Nat. Hazards Earth Syst. Sci.
Discussion started: 12 June 2018

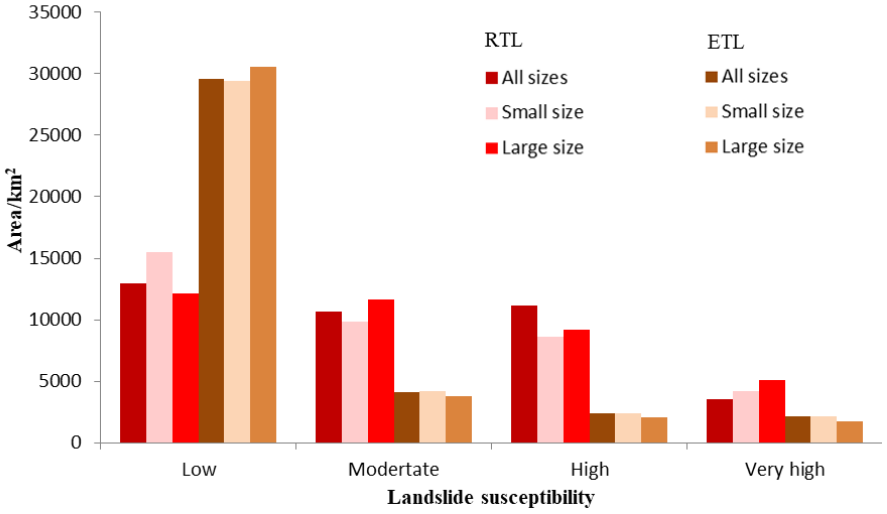

Fig. 7 Statisitcs of areas for different landslide susceptiblity levels on the susceptiblity maps

ROC curves were drawn to verify the accuracy of each susceptiblity model (Fig. 8), and . the Area Under Curve (AUC) was calculated (See Table 2).. The AUC values of the ETL models were higher than for RTL, since the ETL were more concentrated than the RTL, as the inventory is from one single triggering event, whereas the RTLs are from many different rainfall events over a longer time period.

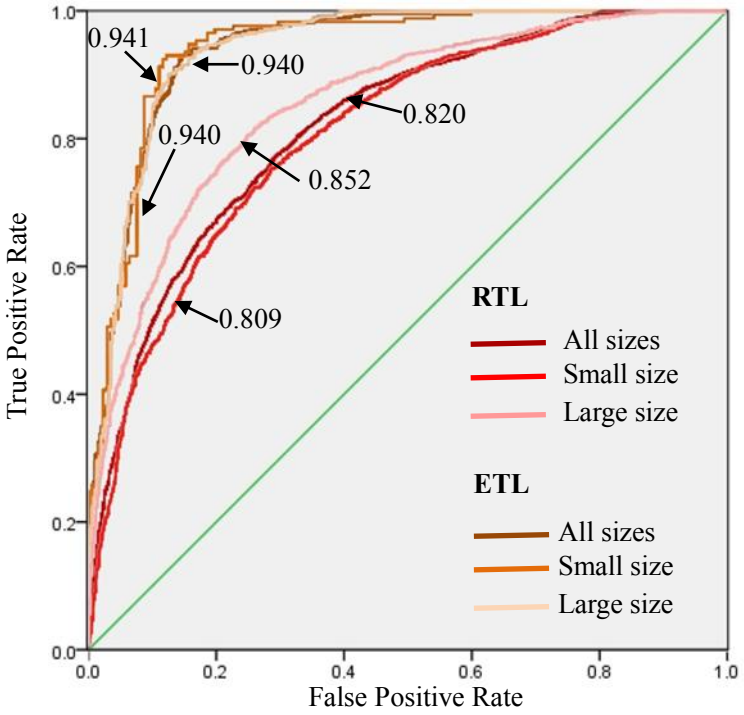

Fig. 8 ROC curves for the susceptibility assessing models to different sizes of RTL and ETL

7. Cross-validation of landslide susceptibility maps

Different groups of landslide data were used to validate the landslide susceptibility maps for RTL and ETL. For each trigger and sizeclass, the number of landslides was calculated, inside the areas with a certain susceptibility level, to cross-validate the results.

a

b

Nat. Hazards Earth Syst. Sci. Discuss., https://doi.org/10.5194/nhess-2018-109
Manuscript under review for journal Nat. Hazards Earth Syst. Sci.
Discussion started: 12 June 2018

Natural Hazards and Earth System Sciences
Discussions

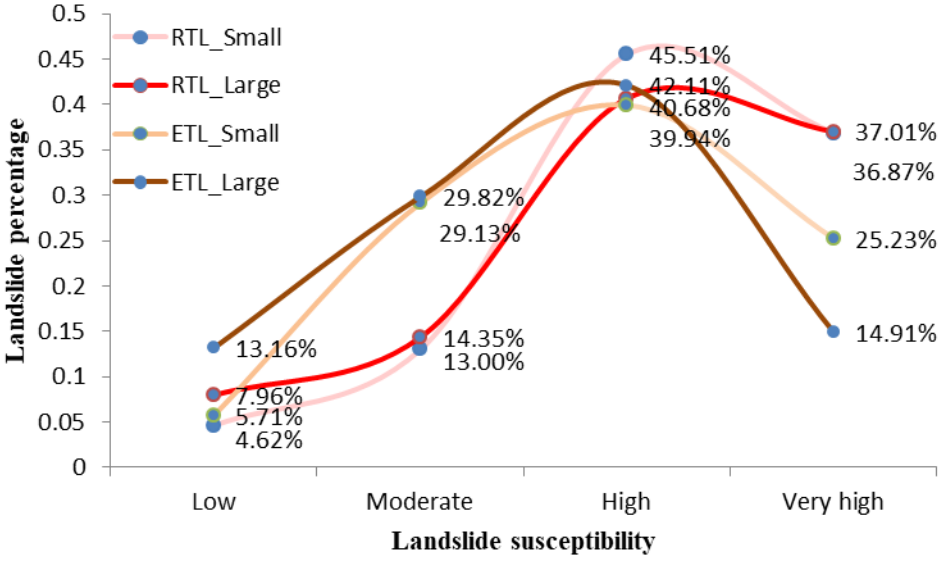

320

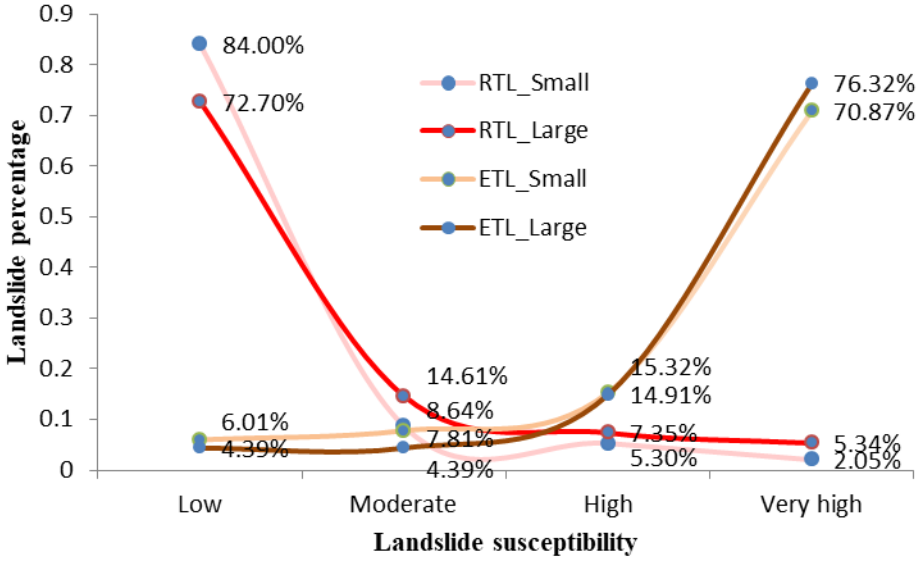

321

322 **Fig. 9** Cross validation of the landslide susceptibility maps. (a) The percentage of landslides in the various classes of
323 the RTL susceptibility map. (b) The percentage of landslides in the various classes of the ETL susceptibility map.

324

325 The percentages of different size RTLs and ETLs in each susceptibility are shown in Fig. 9. For the RTL susceptibility
326 map, percentages of of small size and large size landslides show a similar tendency, for both triggers. More than 40
327 percent of the landslides were located in high susceptibility zones. There is a marked difference between the
328 percentages of ETL and RTL in the ETL landslide susceptibility classes. The RTL are generally much better predicted

than the ETL, of which about 29 % occurs in the moderate class. There is a significant difference in the percentage of landslide sizes for ETL in the low and high susceptibility classes. For ETL there is a difference is the low and very high classes.

For the ETL susceptibility map, the RTL and ETL percentages show completely different patterns. Most of the RTLs (both small and large) are located in the low ETL susceptible regions. Conversely, a large fraction of small size and large size of ETLs are located in the high susceptible regions. The conclusion that can be drawn is that the regions with very high and high suscepbility to ETL are not prone to RTL. This might change however, in the coming period, as the earthquake triggered landslides are bare and often the source of loose debris, that can be reactivated by extreme rainfall events.

8. Discussion and conclusions

This study aimed to analyze independent rainfall- (RTL) and earthquake-triggered landslide (ETL) inventories for a large mountainous watershed in the Himalayas, located in India, Nepal and China. Based on the results of the FAD analysis, the RTL and ETL inventories were subdivided according to landslide size, with a threshold value of 6000 m^2.

The distribution of RTL shows high correlation with altitude and slope aspect due to precipitation. Most of the pre-2015 RTLs are located below 2000 m, and these landslides are more concentrated on south oriented slopes. As the moist airflow from the India Ocean continues to pass over the main crest of the Himalayas, it brings lots of precipitation with increase of altitude, especially on the windward slopes including south, southeast and south west. The high precipitation triggers lots of landslides in these slopes. The airflow loses much of its moisture and warms up as it descends. The rain shadow is formed in the north slopes of the Himalayas, where precipitation rate becomes very low (Zurick and Pacheco 2006). ETL also show different correlation with elevation and aspect. It is more due to the location of epicenter and the propagation direction of seismic wave.

Combination of slope gradient with altitude and lithology affect the size of RTL strongly. There was a clear correlation between the size of the landslides, the slope gradient and altitude. Small RTLs occurred more at lower elevations and less steep slopes relatively, while most large size RTLs are located in higher elevation with steeper slopes. There is no clear differentiation between elevation and slope relations for the two size groups of ETL except in the region with 3500m elevation and 50° slope gradient. ETLs occur more frequently on steeper slopes and in metamorphic rocks than RTLs, which are more prominent in weak sedimentary rocks and colluvium materials.

Weight of landslide susceptibility models can also indicate the significance of causal factors. Altitude, curvature and slope gradient with weights of -7.5456, -6.2341 and 6.1481 respectively have high impact on susceptibility of RTL, while relative relief, curvature and slope gradient with weights of 24.4495, -22.4360 and 8.7348 have high impact on susceptibility of ETL. For different size of RTL and ETL, curvature shows significant different between small size and large size.

The correlation between causal factors and landslide inventories resulted in very different maps for earthquake and rainfall triggered landslides. Most susceptible areas to RTL are located in the Siwalik and Mahabharat Lekh area, with structures oriented in west-east direction, and in the river valleys in the Middle Mountains which are mostly oriented in a north-south direction. ETLs are most likely in the western part of the basin, which is related to the fact that the Gorkha earthquake occurred to the west of the Koshi River basin. The susceptible areas to ETL are much smaller than RTL, and most of them are located on the north, in altitudes between 2000 and 3500 m. The susceptibility map for small size ETL is very similar to the susceptibility map for large size ETL due to the far distance to earthquake epicenter. Some more detail information could be included in large scale research.

The cross-validation showed that the RTL susceptibility map has a modest capability of explaining the ETL pattern, but that the ETL susceptibility cannot properly predict the RTLs. Although landslide size matters, especially for RTLs, there is not such as large difference in behavior for the ETLs. This means one should be careful with using susceptibility maps that were made for earthquake induced landslides, as prediction tools for rainfall induced landslides. Such maps are in fact of little practical implication, as the next earthquake may not be likely to occur in the same location and therefore produce a similar landslide pattern. More advanced methods are required in order to derive earthquake-triggered landslide susceptibility maps, making use of physically-based modelling for many possible earthquake scenarios. Whereas, the use of rainfall-triggered landslide maps can be of some use for predicting the occurrence of earthquake-triggered landslides, one should be careful, as the specific location of the earthquake plays a dominant role. Landslide susceptibility map should also be updated after major earthquakes, as the presence of bare areas with loose debris might trigger more rainfall induced landslides in the years following the earthquake. A major limitation in this work was that we were not able to use separate event-based inventories for RTLs, and only one event-based inventory for ETL. The collection of event-based inventories, both for rainfall and earthquake triggers, remains one of the main challenges in order to advance the study of landslide hazard at a watershed scale.

The Gorkha earthquake triggered a large number of landslides in this basin. Meanwhile the earthquake affected the structure and stability of slopes strongly. So after the earthquake, landslides become more active under the impact of rainfall. What are the characteristics of RTL after earthquake and ETL? Weather there is difference between RTL before earthquake and RTL after earthquake? These could be the further study.

9. Acknowledgements

This research was supported by the National Natural Science Foundation of China (Grant No.41401007), the External Cooperation Program of BIC, Chinese Academy of Sciences (Grant No. 131551KYSB20130003). This study was also jointly supported by the Australian government funded Koshi Basin Programme at ICIMOD as well as ICIMOD's core funds contributed by the governments of Afghanistan, Australia, Austria, Bangladesh, Bhutan, China, India, Myanmar,

Nepal, Norway, Pakistan, Switzerland, and the United Kingdom.

References

Ayalew L, Yamagishi H (2005) The application of GIS-based logistic regression for landslide susceptibility mapping in the Kakuda-Yahiko Mountains, Central Japan. Geomorphology 65(1–2): 15-31, doi:10.1016/j.geomorph.2004.06.010

Bathrellos GD, Kalivas D and Skilodimou HD (2009) GIS-based landslide susceptibility mapping models applied to natural and urban planning in Trikala, Central Greece. Estud Geol 65(1): 49-65. doi: 10.3989/egeol.08642.036

Bai S, Wang J, Lü GN, Zhou PG, Hou SS and Xu SN (2010) GIS-based logistic regression for landslide susceptibility mapping of the Zhongxian segment in the Three Gorges area, China. Geomorphology 115(1–2): 23-31. doi:10.1016/j.geomorph.2009.09.025

Burg JP, Guiraud M, Chen GM, Li GC (1984) Himalayan metamorphism and deformations in the North Himalayan Belt (southern Tibet, China), Earth Planet Sci Lett, 69:391–400.

Carrara A, Cardinali M, Guzzetti F, and Reichenbach P (1995) GIS technology in mapping landslide hazard, In: Carrara A and Guzzetti F (eds), Geographical Information Systems in Assessing Natural Hazards, Kluwer Academic Publishers, Dordrecht, The Netherlands

Chang KT, Chiang SH and Hsu ML (2007) Modeling typhoon- and earthquake-induced landslides in a mountainous watershed using logistic regression. Geomorphology 89(3-4): 335–347. doi:10.1016/j.geomorph.2006.12.011

Chung CJF, Fabbri AG (1993) The representation of geoscience information for data integration. Nonrenewable Resources 2(2): 122–139. doi: 10.1007/BF02272809

Collins BD, Jibson RW (2015) Assessment of existing and potential landslide hazards resulting from the April 25, 2015 Gorkha, Nepal earthquake sequence, U.S. Geological Survey OpenFile Report 2015-1142, Reston, VA

Dai FC, Lee CF (2001) Frequency-volume relation and prediction of rainfall-induced landslides. Engineering Geology 59(3-4): 253-266. doi:10.1016/S0013-7952(00)00077-6

Dahal RK, Hasegawa S (2008) Representative rainfall thresholds for landslides in the Nepal Himalaya. Geomorphology 100 (3-4): 429–443. doi:10.1016/j.geomorph.2008.01.014

Das I, Sahoo S, van Westen CJ, Stain A, Hack R (2000) Landslide susceptibility assessment using logistic regression and its comparison with a rock mass classification system, along a road section in the northern Himalayas (India). Geomorphology 114(4): 627-637, doi:10.1016/j.geomorph.2009.09.023

Dhital MR (2015) Geology of the Nepal Himalaya, Regional Perspective of the Classic Collided Orogen, Springer,

Switzerland. doi:10.1007/978-3-319-02496-7

Dilley M, Chen RS, Deichmann U, Lerner-Lam AL, Arnold M (2005) Natural disaster hotspots: a global risk analysis, The World Bank Hazard Management Unit, Washington

Duman TY, Can T, Gokceoglu C, Nefeslioglu HA, Sonmez H (2006) Application of logistic regression for landslide susceptibility zoning of Cekmece Area, Istanbul, Turkey. Enviromental Geology 51(2): 241-256. doi:10.1007/s00254-006-0322-1

Elliott JR, Jolivet R, González PJ, Avouac J-P, Hollingsworth J, Searle MP, Stevens VL (2016) Himalayan megathrust geometry and relation to topography revealed by the Gorkha earthquake. Nature Geoscience 9:174–180. doi:10.1038/ngeo2623

Gansser A (1964) Geology of the Himalayas, Interscience, New York

Gurung HB and Khanal NR (1987) Landscape processes in the Chure range, Nepal National Committee for Man and the Biosphere, Kathmandu

Guzzetti F, Carrara A, Cardinali M, Reichenbach P (1999) Landslide hazard evaluation: a review of current techniques and their application in a multi-scale study, Central Italy. Geomorphology 31: 181-216, doi:10.1016/S0169-555X(99)00078-1

Guzzetti F, Ardizzone F, Cardinali M, Rossi M, Valigi D (2008) Landslide volumes and landslide mobilization rates in Umbria, central Italy. Earth and Planetary Science Letters 279(3-4): 222-229. doi:10.1016/j.epsl.2009.01.005

Haque U, Blum P, da Silva PF, Andersen P, Pilz J, Chalov SR, Malet J-P, Auflič MJ, Andres N, Royiadji E, Lamas PC, Zhang W, Peshevski I (2016) Fatal landslides in Europe. Landslides 13(6): 1545–1554. doi:10.1007/s10346-016-0689-3

Harp EL, Jibson RW (1996) Landslides triggered by the 1994 Northridge, California earthquake. Bulletin of the Seismological Society of America 86: S319-S332

Hodges KV, Parrish RR, Searle MP (1996) Tectonic evolution of the central Annapurna Range, Nepalese Himalaya, Tectonics, 15:1264–1291

Kamp U, Growley BJ, Khattak GA, Owen LA (2008) GIS-based landslide susceptibility mapping for the 2005 Kashmir earthquake region. Geomorphology 101: 631-642. doi: 10.1016/j.geomorph.2008.03.003

Kargel J, Leonard G, Shugar D. et al. (2016) Geomorphic and geologic controls of geohazards induced by Nepal's 2015 Gorkha earthquake. Science 351(6269), aac8353. doi:10.1126/science.aac8353

Klar A, Aharonow E, Kalderon-Asael B, Katz O (2011) Analytical and observational relations between landslide volume and surface area. Journal of Geophysical Research 116(F2): 1-10. doi:10.1029/2009JF001604

Korup, O., Clague, J.J., Hermanns, R.L., Hewitt, K., Strom, A.L., Weidinger, J.T.（2007）. Giant landslides topography and erosion. Earth Planet. Sci. Lett. 261, 578–589.

456 Larsen IJ, Montgomery DR (2012) Landslide erosion coupled to tectonics and river incision. Nature Geoscience 5(7),
457 468–473. doi:10.1038/ngeo1479
458 Larsen IJ, Montgomery DR, Korup O (2011) Landslide erosion controlled by hillslope material. Nature Geoscience
459 3(4), 247-251. doi:10.1038/ngeo776
460 Peng L, Xu S, Peng J (2014). Research on development characteristics and size of landslide in the Three Gorges area.
461 Geoscience. 28(5): 1077-1086.
462 Lin CW, Liu SH, Lee SY, Liu CC (2006) Impacts of the Chi-Chi earthquake on subsequent rainfall-induced landslides
463 in central Taiwan. Engineering Geology 86(2-3): 87–101. doi:10.1016/j.enggeo.2006.02.010
464 Malamud BD, Turcotte DL, Guzzetti F, Reichenbach P (2004) Landslide inventories and their statistical properties.
465 Earth Surf. Process. Landform 29:687-711. doi:10.1002/esp.1064
466 Martha TR, Reddy PS, Bhatt CM, Govindha Raj KB, Nalini J, Padmanabha A, Narender B, Kumar KV,
467 Muralikrishnan S, Rao GS, Diwakar PG, Dadhwal VK(2017) Debris volume estimation and monitoring of
468 Phuktal river landslide-dammed lake in the Zanskar Himalayas, India using Cartosat-2 images. Landslides
469 14(1): 373-383. doi: 10.1007/s10346-016-0749-8
470 Martha TR, Roy P, Mazumdar R, Govindharaj KB, Kumar KV(2017) Spatial characteristics of landslides triggered by
471 the 2015 Mw 7.8 (Gorkha) and Mw 7.3 (Dolakha) earthquakes in Nepal. Landslides 14(2): 697–704.
472 doi:10.1007/s10346-016-0763-x
473 Menuier P, Hovius N and Haines JA (2008) Topographic site effects and the location of earthquake induced landslides.
474 Earth and Planetary Science Letters 275(3-4): 221-232. doi:10.1016/j.epsl.2008.07.020
475 Nandi A, Shakoor A(2010) A GIS-based landslide susceptibility evaluation using bivariate and multivariate statistical
476 analyses. Engineering Geology 110(1–2): 11-20. doi:10.1016/j.enggeo.2009.10.001
477 Petley D (2012) Global patterns of loss of life from landslides. Geology 40(10): 927–930. doi:10.1130/G33217.1
478 SafeLand (2015) Guidelines for landslide susceptibility, hazard and risk assessment and zoning,
479 https://www.ngi.no/eng/Projects/SafeLand
480 Soeters R, van Westen CJ (1996) Slope instability recognition, analysis, and zonation. In: Turner AK, Schuster
481 RL(eds), Landslides, investigation and mitigation, Washington D.C., National Academy Press
482 Tang C, Zhu J, Qi X (2010) Landslide hazard assessment of the 2008 Wenchuan earthquake: a case study in Beichuan
483 area. Canadian Geotechnical Journal 48(1): 128-145. doi:10.1139/T10-059
484 Tang C, van Westen CJ, Tanyas H, Jetten VG (2016) Analysing post-earthquake landslide activity using multi-
485 temporal landslide inventories near the epicentral area of the 2008 Wenchuan earthquake. Nat. Hazards Earth
486 Syst. Sci. 16: 2641-2655. doi:10.5194/nhess-16-2641-2016
487 Tanyas H, van Westen CJ, Allstadt KE(2017) New method for estimation of landslide-event magnitude based on large

488 dataset of earthquake-induced landslides. Earth Surface Processes and Landforms (Accept)
489 Tong L, Qi S, An G, Liu C (2013) Large scale geo-hazards investigation by remote sensing in Himalayan region,
490 Science Press, Beijing (in Chinese)
491 van Westen CJ, Castellanos E, Kuriakose SL (2008) Spatial data for landslide susceptibility, hazard, and vulnerability
492 assessment: An overview. Eng Geol 102(3-4): 112–131. doi:10.1016/j.enggeo.2008.03.010
493 Wang L, Sawada K, Moriguchi S (2013) Landslide susceptibility analysis with logistic regression model based on
494 FCM sampling strategy. Computers & Geosciences 57: 81-92. doi:10.1016/j.cageo.2013.04.006
495 Xu Q and Li W (2010) Distribution of large-scale landslides induced by the Wenchuan earthquake. Journal of
496 Engineering Geology 18(6) : 818-826(in Chinese)
497 Zhang J, Gurung DR, Liu RK, Murthy MSR, Su FH (2015) Abe Barek landslide and landslide susceptiblity assessment
498 in Badakhshan Province, Afghanistan. Landslides 12(3): 597-609. doi: 10.1007/s10346-015-0558-5
499 Zhang J, Liu R, Deng W, Khanal NR, Gurung DR, Murthy MSR, Wahid S(2016) Characteristics of landslide in Koshi
500 River basin, central Himalaya. Journal of Mountain Science 13(10):1711-1722. doi :10.1007/s11629-016-4017-
501 0
502 Zurick D and Pacheco J (2006) Illustrated atlas of the Himalaya. New Delhi, University Press of Kentucky Lexington
503 and India Research Press

504